

Additional resonant contribution to the potential model for the $^{12}\text{C}(\alpha,\gamma)^{16}\text{O}$ reaction

M. Katsuma

Advanced Mathematical Institute, Osaka City University, Osaka 558-8585, Japan

E-mail: mkatsuma@sci.osaka-cu.ac.jp

Abstract. The additional resonant contribution to the potential model is examined in $\alpha+^{12}\text{C}$ elastic scattering and the low-energy $^{12}\text{C}(\alpha,\gamma)^{16}\text{O}$ reaction. The excitation function of elastic scattering below $E_{c.m.} = 5$ MeV seems to be reproduced by the potential model satisfactorily, and it is not profoundly disturbed by the additional resonances. The weak coupling is good enough to describe the ^{16}O structure in the vicinity of the α -particle threshold, especially below $E_{c.m.} = 8$ MeV, corresponding to the excitation energy $E_x \approx 15$ MeV. The additional resonances give the complement of the astrophysical S -factors from the simple potential model. The S -factor of $^{12}\text{C}(\alpha,\gamma)^{16}\text{O}$ at $E_{c.m.} = 300$ keV is dominated by the $E2$ transition, which is enhanced by the subthreshold 2_1^+ state at $E_x = 6.92$ MeV. The contribution from the subthreshold 1_1^- state at $E_x = 7.12$ MeV is predicted to be small. The additional resonances do not give the large contribution to the thermonuclear reaction rates of $^{12}\text{C}(\alpha,\gamma)^{16}\text{O}$ at helium burning temperatures.

PACS numbers: 25.40.Lw; 24.50.+g; 26.20.Fj

Submitted to: *J. Phys. G: Nucl. Phys.*

1. Introduction

The $^{12}\text{C}(\alpha,\gamma)^{16}\text{O}$ reaction following the triple α reaction in stars plays the very important role in the production of heavier nuclei than carbon [1]. To scrutinize the origin of elements, the low-energy $^{12}\text{C}(\alpha,\gamma)^{16}\text{O}$ cross sections have been investigated at helium burning temperatures, corresponding to the center-of-mass energy $E_{c.m.} \approx 300$ keV. However, the cross sections are very small, owing to the Coulomb barrier, so the direct measurement is not feasible at the present laboratories.

To cope with the difficulty, the theoretical model calculation has been performed with the simple potential model [2, 3]. In this model, $\alpha+^{12}\text{C}$ elastic scattering has been scrutinized to illustrate the feature of the $\alpha+^{12}\text{C}$ continuum state. Below $E_{c.m.} = 5$ MeV, the elastic cross sections have been found to be described very well by the simple $\alpha+^{12}\text{C}$ configuration [3, 4]. The resulting potential between α -particle and ^{12}C nuclei is concordant with the optical model potential reproducing elastic scattering at laboratory energies $E_\alpha \approx 100$ MeV where the ambiguity of the potential is eliminated [5, 6, 7, 8, 9, 10]. The $\alpha+^{12}\text{C}$ rotational bands are well reproduced and the 8^+ and 9^- states at the excitation energy $E_x \approx 30$ MeV are predicted to be the known rotational band member [11, 12]. From the characteristic feature of the reaction mechanism and the ^{16}O structure, the low-energy $^{12}\text{C}(\alpha,\gamma)^{16}\text{O}$ cross sections have been calculated and they have been converted into the astrophysical reaction rates [2, 3]. At $E_{c.m.} = 300$ keV, the radiative capture cross section is dominated by the $E2$ transition to the ground state. The cascade transitions are important above $E_{c.m.} = 1$ MeV, corresponding to $T_9 \approx 1$. T_9 is the temperature in the unit of $T_9 = 10^9$ K. The microscopic models have also attempted to describe the $^{12}\text{C}(\alpha,\gamma)^{16}\text{O}$ reaction and the structure of ^{16}O (e.g. [13]), theoretically.

Recently, the devoted efforts of the progress in the experimental work have been made, as well as the theoretical predictions. At low energies, the γ -ray angular distribution and its ambiguities have been discussed [14, 15, 16, 17, 18]. To cultivate the knowledge of $^{12}\text{C}(\alpha,\gamma)^{16}\text{O}$, the direct measurement of cross sections, the cascade transition through the excited states of ^{16}O and the total capture reaction cross sections have been investigated experimentally (e.g. [19, 20, 21, 22, 23, 24, 25, 26]). However, these measurable energies correspond to the relatively high temperatures, even though they use the current technologies. So, the extrapolated values are made by e.g. the R -matrix method [27]. To pave the way for the analyses, the phase shifts of $\alpha+^{12}\text{C}$ elastic scattering have also been measured precisely [28, 29, 30]. The indirect measurements (e.g. [31, 32]) and the β -delayed α decay of ^{16}N (e.g. [33, 34, 35, 36, 37]) have been demonstrated to evaluate the α -particle width of the subthreshold 1_1^- state ($E_x = 7.12$ MeV), alternatively.

If the radiative capture cross sections are expressed by the Breit-Wigner form, the high energy side of the tail of the subthreshold state could contribute the enhancement of the reaction rates [1, 38]. The low-energy $E1$ cross sections are believed to be enhanced by the 1_1^- state.

Above $E_{c.m.} \simeq 5$ MeV, the $^{15}\text{N}(\text{p},\alpha)^{12}\text{C}$ and the $^{15}\text{N}(\text{p},\gamma)^{16}\text{O}$ reactions are available (e.g. [39, 40, 41, 42, 43, 44, 45, 38]). The branching ratio of these reactions determines the escape from the main CNO cycle to the CNO-II cycle, and it controls the energy production of the proton burning in a star. The low-lying two 1^- resonant states ($E_x = 12.44$ MeV and 13.09 MeV) in the $\text{p}+^{15}\text{N}$ channel appear to be coupled to the $\alpha+^{12}\text{C}$ continuum state. Even at higher energies, the study of the $\alpha+^{12}\text{C}$ system is important in nuclear astrophysics.

In our previous studies [2, 3], we have investigated the $^{12}\text{C}(\alpha,\gamma)^{16}\text{O}$ reaction at sub-barrier energies (below $E_{c.m.} = 3$ MeV), and we have provided the derived reaction rates below $T_9 = 3$. Above the barrier, we see the narrow resonances in the excitation function of elastic scattering (e.g. [46, 47]) and $^{12}\text{C}(\alpha,\gamma)^{16}\text{O}$ (e.g. [19, 21]). The contribution from the resonances has not been explicitly discussed yet. At $T_9 = 3$, the so-called Gamov peak energy E_0 and width ΔE_0 [1, 38] are $E_0 = 1.92$ MeV and $\Delta E_0 = 1.63$ MeV, respectively. If taking account of the numerical integration up to $E_0 + 3\Delta E_0 = 6.8$ MeV [38], we might want to discuss the contribution from the cross sections above the barrier.

In the present article, we investigate the additional resonant contribution to the potential model for $\alpha+^{12}\text{C}$ elastic scattering and the $^{12}\text{C}(\alpha,\gamma)^{16}\text{O}$ reaction. We show whether the potential model reproduces the excitation function of $\alpha+^{12}\text{C}$ elastic scattering and the astrophysical S -factors, including the known resonances. We estimate the difference in the derived reaction rates below $T_9 = 3$. The contribution from the subthreshold states is also discussed. The main purpose of the present study is to examine the additional resonant contribution to the calculated cross sections and reaction rates.

In the following section, we explain the potential model with the additional resonances. In Section 3, the contribution from the additional resonances is discussed by showing the difference in the excitation function of $\alpha+^{12}\text{C}$ elastic scattering and the $^{12}\text{C}(\alpha,\gamma_0)^{16}\text{O}$ S -factors. The derived reaction rates are also compared with the previous ones [2]. The summary is given in Section 4.

2. Potential model with the additional resonances

In this section, we describe the potential model [2, 3, 48, 49]. The basic idea of the potential model is based on the mean field approximation of quantum many-body systems [10]. The potential model describes relative motion between interacting two nuclei, and it makes the potential resonance and the smooth variation on energy in the excitation function. The narrow resonances are appended to the result obtained from the simple potential model. We refer the simple potential model calculation without the additional resonances as the direct-capture component or potential scattering in the present article. The additional resonant term is called the resonant component or dynamical process, because it originates from the couplings to other reaction channels.

The astrophysical S -factors for the radiative capture reaction are conventionally

used instead of the cross sections to compensate for the rapid drop of the cross sections below the barrier [1, 38, 50], and they are defined by

$$S_{E\lambda}(E_{c.m.}) = E_{c.m.} \exp(2\pi\eta) \sigma_{E\lambda}(E_{c.m.}), \quad (1)$$

where η is the Sommerfeld parameter, $\eta = Z_1 Z_2 e^2 / (\hbar v)$; $v = \sqrt{2E_{c.m.}/\mu}$; Z_1 and Z_2 are the charge of α -particle and ^{12}C ; μ is the reduced mass. λ is multipole of the transition. $\sigma_{E\lambda}(E_{c.m.})$ is the radiative capture cross section, defined by

$$\sigma_{E\lambda}(E_{c.m.}) = \sum_f \frac{2J_f + 1}{(2I_1 + 1)(2I_2 + 1)} \frac{\pi}{k_i^2} \sum_{l_i} |T_{l_f l_i}^{E\lambda}(k_f, k_i)|^2. \quad (2)$$

J_f is the spin of the final bound state; I_1 and I_2 are the spin of interacting two nuclei. k and l are the wave number and the angular momentum of relative motion between α and ^{12}C . The subscript denotes the value for the initial channel (i) and final state (f).

The transition amplitudes $T_{l_f l_i}^{E\lambda}(k_f, k_i)$ is defined by

$$T_{l_f l_i}^{E\lambda}(k_f, k_i) = \bar{T}_{l_f l_i}^{E\lambda}(k_f, k_i) - i \sum_n \tilde{e}_{E\lambda} \frac{\sqrt{\Gamma_{\gamma n} \Gamma_{\alpha n}}}{E_{c.m.} - E_n + i\Gamma_n/2}, \quad (3)$$

where E_n , $\Gamma_{\alpha n}$, $\Gamma_{\gamma n}$ and Γ_n are the resonance energy, the α -particle width, the γ -width and total width of the resonance n , respectively. The first term represent the direct-capture component. For $^{12}\text{C}(\alpha, \gamma_0)^{16}\text{O}$, the direct-capture component is given by

$$\bar{T}_{0l_i}^{E\lambda}(k_f, k_i) = \tilde{e}_{E\lambda} C_\lambda \left[\frac{8\pi(\lambda + 1)k_\gamma^{2\lambda+1}}{\hbar v \lambda [(2\lambda + 1)!!]^2} \right]^{1/2} \int \chi_{f,0}(k_f r) r^\lambda \chi_{i,l_i}(k_i r) dr, \quad (4)$$

where C_λ is the geometric factor. $\tilde{e}_{E\lambda}$ is the effective charge for $E\lambda$ transition, which is determined from the direct-capture component. k_γ is the wave number of the emitted γ -rays, $k_\gamma = (E_{c.m.} - E_f)/(\hbar c)$. E_f is the binding energy of the final state. $\chi_{i,f}$ is the wavefunction of relative motion obtained from solving the Schrödinger equation with the local potential. We adopt the parity-dependent nuclear potential,

$$V(r) = \begin{cases} V_+ f_+(r) & (\text{even}) \\ V_- f_-(r) & (\text{odd}) \end{cases}, \quad (5)$$

$$f_\xi(r) = \frac{1}{1 + \exp[(r - R_\xi)/a_\xi]}. \quad (6)$$

V_ξ , R_ξ and a_ξ are the potential parameters for the even (+) and odd (-) parities. We use the same parameters as those in the previous studies [2, 3, 4]: $V_+ = -199.7$ MeV, $R_+ = 2.18$ fm, $a_+ = 0.743$ fm, $V_- = -168.1$ MeV, $R_- = 2.76$ fm, and $a_- = 0.567$ fm for $\alpha + ^{12}\text{C}$ continuum state. The V_+ is adjusted to reproduce the α -particle separation energy for the ground state. The Coulomb potential is calculated from the uniform charge sphere with a radius $R_C = 3.5$ fm. The $E1$ and $E2$ effective charges are $\tilde{e}_{E1} = 9.96 \times 10^{-3}e$ and $\tilde{e}_{E2} = 1.69e$ [3]. $\tilde{e}_{E1} = 0.68e$ [3] is used for the resonance at $E_n = 5.928$ MeV.

The nuclear reactions proceed in the sequence of elastic scattering, direct reactions and more complicated nuclear reactions [10]. The direct-capture component describes the fundamental process of the radiative capture reactions. The more complicated

reaction process occurs after the direct-capture process with penetrating the barrier. In equation (3), the Breit-Wigner form is attached to include the dynamical process. The included resonances are listed in Table 1. The $0^+(E_{c.m.} = -1.113 \text{ MeV})$, $1^-(E_{c.m.} = 2.42 \text{ MeV})$, $2^+(E_{c.m.} = -0.245 \text{ MeV})$, $3^-(E_{c.m.} = 4.44 \text{ MeV})$, $4^+(E_{c.m.} = 3.19 \text{ MeV})$ and $5^-(E_{c.m.} = 7.50 \text{ MeV})$ states are not included as the additional resonances. These are generated by the potential resonance.

In the present work, we do not perform the χ^2 optimization to the experimental data. The purpose of the present article is to illustrate the contribution from the additional resonances, in comparison with the direct-capture component of our previous studies [2, 3].

For elastic scattering, we utilize the dispersion formula of the S -matrix.

$$\mathcal{S}_L = \bar{\mathcal{S}}_L - i \sum_n \frac{\Gamma_{\alpha n} e^{i\theta_{\alpha n}}}{E_{c.m.} - E_n + i\Gamma_n/2}, \quad (7)$$

where $\bar{\mathcal{S}}_L$ is the S -matrix from potential scattering. The second term is the dynamical component. $\theta_{\alpha n} = 2\bar{\delta}_i$ is used. $\bar{\delta}_i$ is the phase shifts of potential scattering. The excitation function of elastic scattering is calculated from equation (7).

From the energy dependence of wavefunctions at low energies, the α -particle width is assumed to be given by attaching a factor to the energy-independent experimental value [1, 38],

$$\Gamma_{\alpha n}(E_{c.m.}) = \frac{P(E_{c.m.})}{P(|E_n|)} \Gamma_{\alpha n}. \quad (8)$$

$P(E_{c.m.})$ is defined by the Gamov factor,

$$P(E_{c.m.}) = \exp[-2\pi\eta(E_{c.m.})]. \quad (9)$$

$\eta(|E_n|) = -\eta(|E_n|)$ is assumed to be used for the negative energy. The energy dependence of γ -width comes from the wavelength of the emitted γ -rays,

$$\Gamma_{\gamma n}(E_{c.m.}) = \left(\frac{E_{c.m.} - E_f}{E_n - E_f} \right)^{2\lambda+1} \Gamma_{\gamma n}. \quad (10)$$

The Maxwellian-averaged reaction rates $N_A \langle \sigma v \rangle$ [1, 38, 50] are converted from the calculated S -factors.

$$N_A \langle \sigma v \rangle = N_A \frac{(8/\pi)^{1/2}}{\mu^{1/2} (k_B T)^{3/2}} \int \sigma_{E\lambda}(E_{c.m.}) E_{c.m.} \exp\left(-\frac{E_{c.m.}}{k_B T}\right) dE_{c.m.}, \quad (11)$$

where N_A , k_B , and T are the Avogadro number, Boltzmann constant and temperature, respectively. The S -factors consist of the direct-capture and dynamical components. So, the additional resonances increase the reaction rates from the previous ones [2].

In addition, we estimate the reaction rates from the resonances by using the formula [1, 38, 50],

$$N_A \langle \sigma v \rangle_R = N_A \left(\frac{2\pi}{\mu k_B} \right)^{3/2} \hbar^2 \sum_n (\omega\gamma)_n T^{-3/2} \exp(-E_n/k_B T) + N_A \left(\frac{2}{\mu} \right)^{1/2} \cdot \frac{\Delta E_0}{(k_B T)^{3/2}} \sum_n S_n(E_0) \exp \left[-3 \left(\frac{\pi^2 \mu}{2k_B T} \right)^{1/3} \left(\frac{e^2 Z_1 Z_2}{\hbar} \right)^{2/3} \right], \quad (12)$$

where $(\omega\gamma)_n$ is given by

$$(\omega\gamma)_n = \frac{\Gamma_{\gamma 0n} \Gamma_{\alpha n}}{\Gamma_n}. \quad (13)$$

$S_n(E_0)$ is the S -factor of the resonance n . E_0 and ΔE_0 are given by $E_0 \approx 0.922T_9^{2/3}$ and $\Delta E_0 \approx 0.651T_9^{5/6}$, respectively. The formula of equation (12) is utilized in general to estimate roughly the reaction rates although it does not include the interference between the resonances. When it is compared with the numerical integration of equation (11), the direct-capture component is added to equation (12).

3. Results

In this section, we examine the additional resonant contribution to the potential model for $\alpha+^{12}\text{C}$ elastic scattering and $^{12}\text{C}(\alpha,\gamma)^{16}\text{O}$. We compare the calculated results of the excitation function and the phase shifts with those [4] from potential scattering below $E_{c.m.} = 5$ MeV. After illustrating the applicability of the model, we discuss the effect to the astrophysical S -factor of the $^{12}\text{C}(\alpha,\gamma)^{16}\text{O}$ reaction. Using the $E2$ transition, we recall the tail contribution of the subthreshold state in the S -factors. We explain the contribution from the additional subthreshold 1_1^- state, which is not included explicitly in the potential model with the simple $\alpha+^{12}\text{C}$ configuration. We finally estimate the additional contribution to the derived reaction rates below $T_9 = 3$.

3.1. $\alpha+^{12}\text{C}$ elastic scattering

Figure 1 shows the excitation function of $\alpha+^{12}\text{C}$ elastic scattering below $E_{c.m.} = 5$ MeV for (a) $\theta_{c.m.} = 36.9^\circ - 111.2^\circ$ and (b) $\theta_{c.m.} = 121.8^\circ - 168.5^\circ$. The solid curves are the calculated results with the additional resonances. The dotted curves are obtained from potential scattering [4]. At $E_{c.m.} \approx 4.4$ MeV, we see the difference between two curves due to the 2_3^+ resonance at $E_{c.m.} = 4.357$ MeV ($E_x = 11.52$ MeV). We also see the small peak at $E_{c.m.} \approx 2.683$ MeV, which originates from the 2_2^+ narrow resonance. It is, however, found that the additional resonances give no more than the slight deviation from potential scattering. The arrows indicate the energy position of the states belonging to the rotational bands [11, 12]. From the comparison between two curves, the weak coupling is confirmed to be good enough to describe the excitation function below $E_{c.m.} = 5$ MeV.

The corresponding phase shifts for (a) $l_i = 0, 2, 4$ and (b) $l_i = 1, 3$ are shown in figure 2. The solid and dotted curves are the results with/without the additional resonances. The $l_i = 2$ phase shift has the step of 180° because of the 2_2^+ ($E_{c.m.} = 2.683$ MeV) and 2_3^+ ($E_{c.m.} = 4.357$ MeV) resonances. However, the difference of the $l_i = 2$ phase shift is localized around the resonance energies because $\delta_{l_i} = 0$ is equal to $\delta_{l_i} = 180$. The difference in the phase shifts reflects to the deviation between two curves of the excitation function shown in figure 1. We figure out that the additional resonances do not contribute to elastic scattering below $E_{c.m.} = 5$ MeV, substantially.

To verify that the present model is suitable above the barrier, we illustrate the excitation function of $\alpha+^{12}\text{C}$ elastic scattering up to $E_{c.m.} = 8$ MeV, as well. The solid and dotted curves in figure 3 are the results obtained from the potential model with/without the additional resonances. The characteristic feature of the experimental data appears to be reproduced by the solid curves. The potential scattering shown by the dotted curves seems to give the smooth trend of the excitation function and the potential resonances. The remaining rapid variations come from the additional resonances (Table 1). The strength of the potential for $l_i = 5$ is slightly adjusted as $V_{l=5} = -170.3$ MeV so as to reproduce the experimental $l_i = 5$ resonance. From the comparison between two curves, we find that the weak coupling is still appropriate for describing the outline of the $\alpha+^{12}\text{C}$ excitation function up to $E_{c.m.} = 8$ MeV. We here confirm that the excited states of ^{16}O nuclei below $E_x \approx 15$ MeV are described by the present model.

3.2. Astrophysical S -factors

The calculated S -factors are compared in figure 4. The solid curve is the result obtained from the potential model with the additional resonances, and it is the sum of the S -factors of the $E1$ and $E2$ transitions to the ground state of ^{16}O . The dotted curves are the direct-capture component. We see the large difference because of the resonances at $E_{c.m.} = 4.357$ MeV, 5.865 MeV and 5.928 MeV. The narrow resonance makes the sharp peak at $E_{c.m.} = 2.683$ MeV. We, however, find that the S -factors are not disturbed by the additional resonances below $E_{c.m.} = 3$ MeV. The small deviation makes us expect that the additional resonances do not give the profound change of the reaction rates below $T_9 \approx 3$. The S -factors at low energies are dominated by the $E2$ transition in the potential model, as discussed in [2, 3].

Before discussing the subthreshold 1_1^- state, let us explain how the subthreshold 2_1^+ state dominates the S -factor at $E_{c.m.} = 300$ keV. Figure 5 shows the schematic calculation of the $E2$ S -factors. The strength of the even-parity potential V_+ is varied. If the attraction of the nuclear potential V_+ becomes weaker, the sharp peak appears at low energies. And the peak energy is shifted higher as V_+ is getting weak. The shape of the resonance is not changed in the S -factors. This means that the resonant peak is the 2_1^+ bound state emerging from beneath the threshold. From figure 5, we confirm that the $E2$ S -factors are enhanced by the the subthreshold 2_1^+ state.

In contrast, the $E1$ S -factors are not enhanced by the subthreshold 1_1^- state in the simple potential model [2, 3]. The solid curve in figure 6 is the $E1$ S -factors obtained from the potential model with the additional resonances. The dashed curves represent the component of the additional resonances. From this figure we find that the low-energy S -factors are not enhanced by the subthreshold 1_1^- state. In the present model, the α -particle width of the 1_1^- state at low energies is reduced by $P(|E_R|)$, even if we surmise $\Gamma_{\alpha n}$ in equation (8). We also find, from the comparison between two curves, that the direct-capture component dominates the $E1$ S -factors below $E_{c.m.} = 3$ MeV.

As an examination, we introduce the reduced width γ_α^2 with the assumed channel radius a_c , in accordance with the R -matrix method. Instead of equation (8), we use the α -particle width, defined by

$$\Gamma_\alpha(E_{c.m.}) = 2P_L(E_{c.m.})\gamma_\alpha^2, \quad (14)$$

for the subthreshold 1_1^- state. γ_α^2 is defined by the probability of α -particle at the channel radius a_c . $P_L(E_{c.m.})$ is given by

$$P_L(E_{c.m.}) = \begin{cases} \frac{k_i a_c}{G_L^2(k_i a_c) + F_L^2(k_i a_c)} & (E_{c.m.} > 0) \\ 0 & (E_{c.m.} \leq 0) \end{cases}, \quad (15)$$

where $F_L(k_i a_c)$ and $G_L(k_i a_c)$ are the regular and irregular Coulomb wave functions, respectively. $P_L(E_{c.m.})$ varies as equation (9) at low energies, $k_i a_c \approx 0$. The dotted curve in figure 6 is calculated from equations (14) and (15) and $\gamma_\alpha^2 = 2.97$ keV [51] for the 1_1^- state. $a_c = 6.5$ fm is used. If we use the width as in the R -matrix method, we find the tail of the subthreshold state at low energies. It however does not strongly interfere with the direct-capture component. We thus figure out that the resulting total $E1$ S -factor with equations (14) and (15) is almost identical to the result with equation (9).

The $E1$ transition is hindered by the isospin selection rule [52], and the absolute value of the $E1$ S -factors is reduced at low energies. Under the weak coupling, the additional narrow resonance cannot interfere with the 1_2^- state ($E_{c.m.} = 2.42$ MeV) belonging to the $\alpha+^{12}\text{C}$ rotational band which has the relatively large amplitude. We also predict, for the same reason, that the S -factor of the 1_3^- state at $E_{c.m.} = 5.282$ MeV ($E_x = 12.44$ MeV) is reduced if we use the given resonance width [46].

In the R -matrix analyses, the *transparent* feature of the reactions is not taken into account. The ^{16}O structure described by the relative motion between α -particle and ^{12}C might not be considered correctly. The large violation of the isospin selection rule is surmised to be allowed in the *internal* region.

The resulting S -factors at $E_{c.m.} = 300$ keV are $S_{E1} \approx 3$ keV b and $S_{E2} = 152$ keV b, respectively. They are approximately the same as our previous values [3].

3.3. $^{12}\text{C}(\alpha,\gamma)^{16}\text{O}$ reaction rates

Figure 7 compare the derived reaction rates with our recommended reaction rates (KA12) in [2]. The solid curve is the result displayed in the ratio to KA12. The difference from unity indicates the contribution of the additional resonances in the present calculation. The shade region is the uncertainties estimated from the variation of the model parameters [2]. We find, from the figure, that the additional resonances do not make the profound change in the reaction rates below $T_9 = 3$. They produce the difference below 5 %. The dotted curve represents the reaction rates with equation (12). We find that the resonant component from equation (12) is very small. The dotted curve does not include the interference between the resonances and the direct-capture component. So, the increase in the reaction rate of the solid curve is caused by the weak interference between the components, rather than the resonant peak. The

numerical integration of equation (11) below $T_9 = 3$ is in convergence at $E_{c.m.} = 7$ MeV, satisfactorily.

From figure 7, we also find that the uncertainties of the reaction rates still remain at high temperatures, $T_9 > 1$. The primary reason of the uncertainties comes from the cascade transition through the excited state of ^{16}O , as discussed in [2, 3]. They will be discussed in detail in the forthcoming paper.

4. Summary

We have examined the additional resonant contribution to the potential model for the $^{12}\text{C}(\alpha,\gamma)^{16}\text{O}$ reaction. We have calculated the excitation function of $\alpha+^{12}\text{C}$ elastic scattering below $E_{c.m.} = 8$ MeV, the low-energy astrophysical S -factors and the reaction rates of $^{12}\text{C}(\alpha,\gamma)^{16}\text{O}$ below $T_9 = 3$. In the present calculation, we use the parity-dependent real potential and include the known resonances as the Breit-Wigner form.

The excitation functions and phase shifts of $\alpha+^{12}\text{C}$ elastic scattering below $E_{c.m.} = 5$ MeV seem to be satisfactorily reproduced. The potential scattering appears to give the smooth trend of the excitation function and the single-particle potential resonances below $E_{c.m.} = 8$ MeV. The remaining rapid variation on the excitation function originates from the additional resonances. From the comparison, we find that the weak coupling to other reaction channels is good enough to describe in outline the structure of ^{16}O below $E_x \approx 15$ MeV.

The additional resonances complement the astrophysical S -factors obtained from the potential model. However, they do not give the large contribution to the derived $^{12}\text{C}(\alpha,\gamma)^{16}\text{O}$ reaction rates below $T_9 = 3$. (below 5%) The S -factor at $E_{c.m.} = 300$ keV is dominated by the $E2$ transition because of the subthreshold 2_1^+ state. The $E1$ is not enhanced by the subthreshold 1_1^- state. The S -factors at $E_{c.m.} = 300$ keV are found to be $S_{E1} \approx 3$ keV b and $S_{E2} = 152$ keV b, and they are approximately the same as the results of [3]. The simple potential model [3] describes the fundamental process of the radiative capture reactions. Compared with the direct-capture component, the additional $E1$ resonant component is small, and it does not strongly couple to the direct-capture process at low energies.

Acknowledgments

The author thanks Professors K. Langanke, G. Martínez-Pinedo, and I.J. Thompson for their comments and hospitality during his visiting program. He also thanks Professors Y. Ohnita and Y. Sakuragi for their hospitality and encouragement and Professor Y. Kondō for the early days of the collaboration. He is grateful to Professors M. Arnould, A. Jorissen, K. Takahashi, and H. Utsunomiya for their hospitality during his stay at Université Libre de Bruxelles (ULB). The part of this work has been supported by the Interuniversity Attraction Pole IAP 5/07 of the Belgian Federal Science Policy (Konan University – ULB convention), and by the JSPS Institutional Program for Young

Researcher Overseas Visits “Promoting international young researchers in mathematics and mathematical sciences led by Osaka City University Advanced Mathematical Institute”.

References

- [1] Rolfs C E and Rodney W S 1988 *Cauldrons in the Cosmos* (Chicago: The University of Chicago Press)
- [2] Katsuma M 2012 *Astrophys. J.* **745** 192
- [3] Katsuma M 2008 *Phys. Rev. C* **78** 034606
- [4] Katsuma M 2010 *Phys. Rev. C* **81** 067603
- [5] Ingemarsson A, Auce A and Johansson R 1994 *Phys. Rev. C* **49** 1609
- [6] Nolte M, Machner H and Bojowald J 1987 *Phys. Rev. C* **36** 1312
- [7] Michel F, Reidemeister G and Kondō Y 1995 *Phys. Rev. C* **51** 3290
- [8] Michel F, Albinski J, Belery P *et al.* 1983 *Phys. Rev. C* **28** 1904
- [9] Brandan M E and Satchler G R 1997 *Phys. Rep.* **285** 143
- [10] Satchler G R 1983 *Direct Nuclear Reactions* (International series of monographs on physics) (New York: Oxford University Press)
- [11] Katsuma M 2014 *EPJ Web of Conferences* **66** 03041
- [12] Katsuma M 2013 *J Phys. G* **40** 025107
- [13] Dufour M and Descouvemont P 2008 *Phys. Rev. C* **78** 015808
- [14] Gai M 2013 *Phys. Rev. C* **88** 062801
- [15] Plag R, Reifarh R, Heil M *et al.* 2012 *Phys. Rev. C* **86** 015805
- [16] Makii H, Nagai Y, Shima T *et al.* 2009 *Phys. Rev. C* **80** 065802
- [17] Assunção M, Fey M, Lefebvre-Schuhl A *et al.* 2006 *Phys. Rev. C* **73** 055801
- [18] Kunz R, Jaeger M, Mayer A *et al.* 2001 *Phys. Rev. Lett.* **86** 3244
- [19] Schürmann D, Gialanella L, Kunz R, Strieder F 2012 *Phys. Lett. B* **711** 35
- [20] Schürmann D, Di Leva A, Gialanella L *et al.* 2011 *Phys. Lett. B* **703** 557
- [21] Schürmann D, Di Leva A, Gialanella L *et al.* 2005 *Eur. Phys. J. A* **26** 301
- [22] Matei C, Buchmann L, Hannes W R *et al.* 2006 *Phys. Rev. Lett.* **97** 242503
- [23] Kunz R, Fey M, Jaeger M *et al.* 2002 *Astrophys. J.* **567** 643
- [24] Roters G, Rolfs C, Strieder F, Trautvetter H P 1999 *Eur. Phys. J. A* **6** 451
- [25] Redder A, Becker H W, Rolfs C *et al.* 1987 *Nucl. Phys. A* **462** 385
- [26] Kettner K U, Becker H W, Buchmann L *et al.* 1982 *Z. Phys. A* **308** 73
- [27] Lane A M and Thomas R G 1958 *Rev. Mod. Phys.* **30** 257
- [28] Tischhauser P, Couture A, Detwiler R *et al.* 2009 *Phys. Rev. C* **79** 055803
- [29] Tischhauser P, Azuma R E, Buchmann L *et al.* 2002 *Phys. Rev. Lett.* **88** 072501
- [30] Plaga R, Becker H W, Redder A *et al.* 1987 *Nucl. Phys. A* **465** 291
- [31] Brune C R, Geist W H, Kavanagh R W *et al.* 1999 *Phys. Rev. Lett.* **83** 4025
- [32] Belhout A, Ouichaoui S, Beaumeville H *et al.* 2007 *Nucl. Phys. A* **793** 178
- [33] Tang X D, Rehm K E, Ahmad I *et al.* 2010 *Phys. Rev. C* **81** 045809
- [34] Buchmann L R and Barnes C A 2006 *Nucl. Phys. A* **777** 254
- [35] Buchmann L, Azuma R E, Barnes C A *et al.* 1996 *Phys. Rev. C* **54** 393
- [36] Azuma R E, Buchmann L, Barker F C *et al.* 1994 *Phys. Rev. C* **50** 1194
- [37] Buchmann L, Azuma R E, Barnes C A *et al.* 1993 *Phys. Rev. Lett.* **70** 726
- [38] Angulo C, Arnould M, Rayet M *et al.* 1999 *Nucl. Phys. A* **656** 3
- [39] La Cognata M, Romano S, Spitaleri C *et al.* 2007 *Phys. Rev. C* **76** 065804
- [40] La Cognata M, Goldberg V Z, Mukhamedzhanov A M *et al.* 2009 *Phys. Rev. C* **80** 012801
- [41] Barker F C 2008 *Phys. Rev. C* **78** 044611
- [42] Marta M, Trompler E, Bemmerer D *et al.* 2010 *Phys. Rev. C* **81** 055807

- [43] Imbriani G, deBoer R J, Best A *et al.* 2012 *Phys. Rev. C* **85** 065810
- [44] Imbriani G, deBoer R J, Best A *et al.* 2012 *Phys. Rev. C* **86** 039902
- [45] Rolfs C and Rodney W 1974 *Nucl. Phys. A* **235** 450
- [46] Tilley D R, Weller H R and Cheves C M 1993 *Nucl. Phys. A* **564** 1
- [47] Marvin T P and Singh P P 1972 *Nuclear Physics A* **180** 282
- [48] Descouvemont P 2003 *Theoretical Models for Nuclear Astrophysics* (New York: Nova Science Publishers)
- [49] Rose H J and Brink D M 1967 *Rev. Mod. Phys.* **39** 306
- [50] Fowler W, Caughlan G and Zimmerman B 1967 *Ann. Rev. Astron. Astrophys.* **5** 525
- [51] Xu Y, Takahashi K, Goriely S, Arnould M *et al.* 2013 *Nucl. Phys. A* **918** 61
- [52] Eisenberg J M and Greiner W 1976 *Nuclear theory, vol. 2, revised edition* (Amsterdam: North-Holland Publishing company)
- [53] Firestone R B, Shirley V S, Baglin C M *et al.* 1996 *Table of Isotopes 8th Edition* Lawrence Berkeley National Laboratory, University of California (New York: John Wiley & Sons, Inc.)
- [54] International Network of Nuclear Reaction Data Centres, *Experimental Nuclear Reaction Data (EXFOR)*

Tables and table captions

Table 1. The $\alpha+^{12}\text{C}$ resonant states of ^{16}O [46, 47, 53] attached in the present calculation. The resonance energy E_n , the α -particle width $\Gamma_{\alpha n}$, the γ -width to the ground state $\Gamma_{\gamma_0 n}$, and the total width Γ_n are listed. E_n is given in the center-of-mass energy. $\Gamma_{\alpha n}$ is indicated in the ratio to Γ_n .

n	E_n (MeV)	J^π	Γ_n (keV)	$\Gamma_{\alpha n}/\Gamma_n$	$\Gamma_{\gamma_0 n}$ (eV)
1	-0.045	1^-	—	—	7.9×10^{-2}
2	2.683	2^+	0.625	1.0	5.7×10^{-3}
3	3.934	4^+	0.28	1.0	—
4	4.357	2^+	73.	1.0	0.65
5	4.889	0^+	1.5	1.0	—
6	5.282	1^-	99.	0.93	9.5
7	5.865	2^+	150.	1.0	0.7
8	5.928	1^-	130.	0.35	44.0
9	5.970	3^-	110.	0.82	—
10	6.098	3^-	26.	0.35	—
11	6.720	4^+	75.	0.65	—
12	6.873	0^+	200.	1.0	—
13	6.975	3^-	750.	0.20	—
14	7.461	4^+	487.	0.80	—
15	7.646	6^+	70.	0.31	—
16	7.908	0^+	166.	0.80	—
17	8.249	3^-	133.	0.58	—

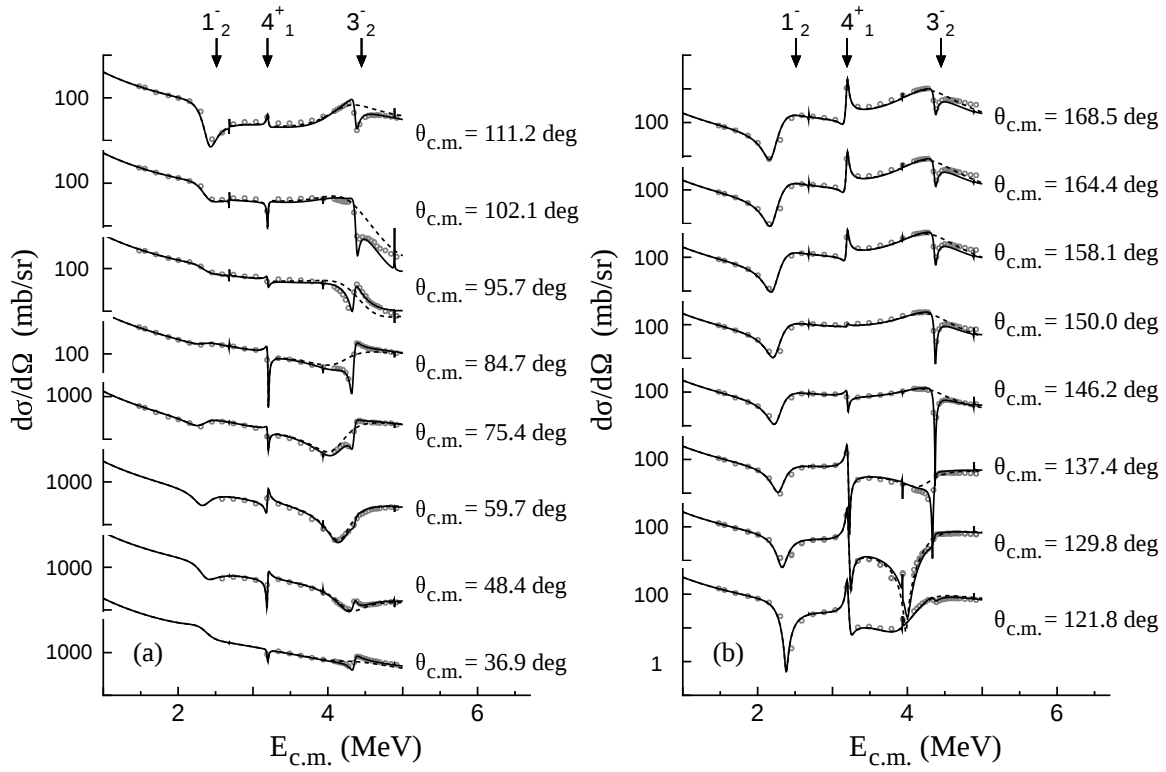


Figure 1. The excitation function of $\alpha + ^{12}\text{C}$ elastic scattering below $E_{c.m.} = 5$ MeV. The solid curves are the results obtained from the potential model with the additional resonances. The dotted curves represent the results from potential scattering. The energy position of the $\alpha + ^{12}\text{C}$ rotational band [11, 12] is shown by the arrows. The scattering angles are displayed besides the respective curves. The experimental data are taken from [30, 54].

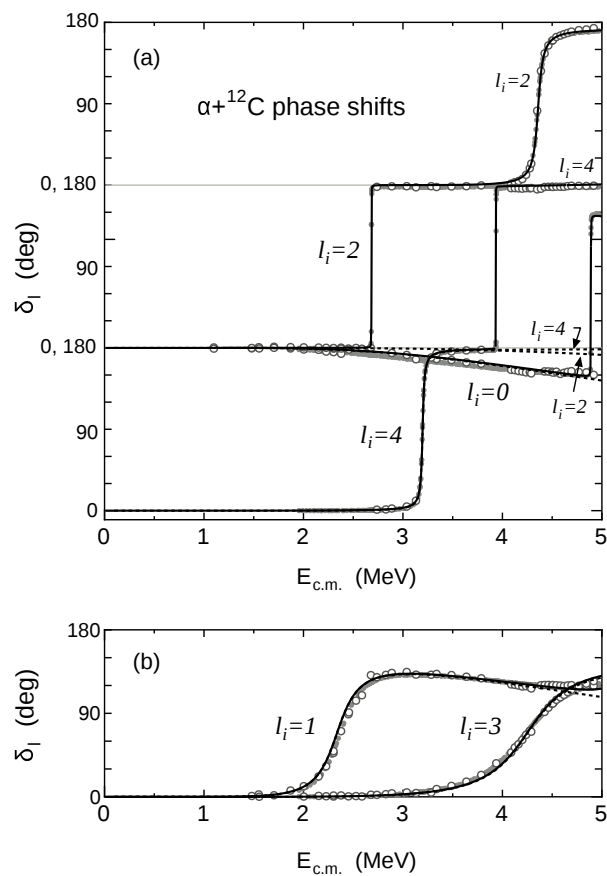


Figure 2. The phase shifts of (a) $l_i = 0, 2$ and 4 (b) $l_i = 1$ and 3 for $\alpha + ^{12}\text{C}$ elastic scattering. The solid curves are the calculated phase shifts with the additional resonances. The dotted curves represent the results from potential scattering. The experimental data are taken from [30, 28].

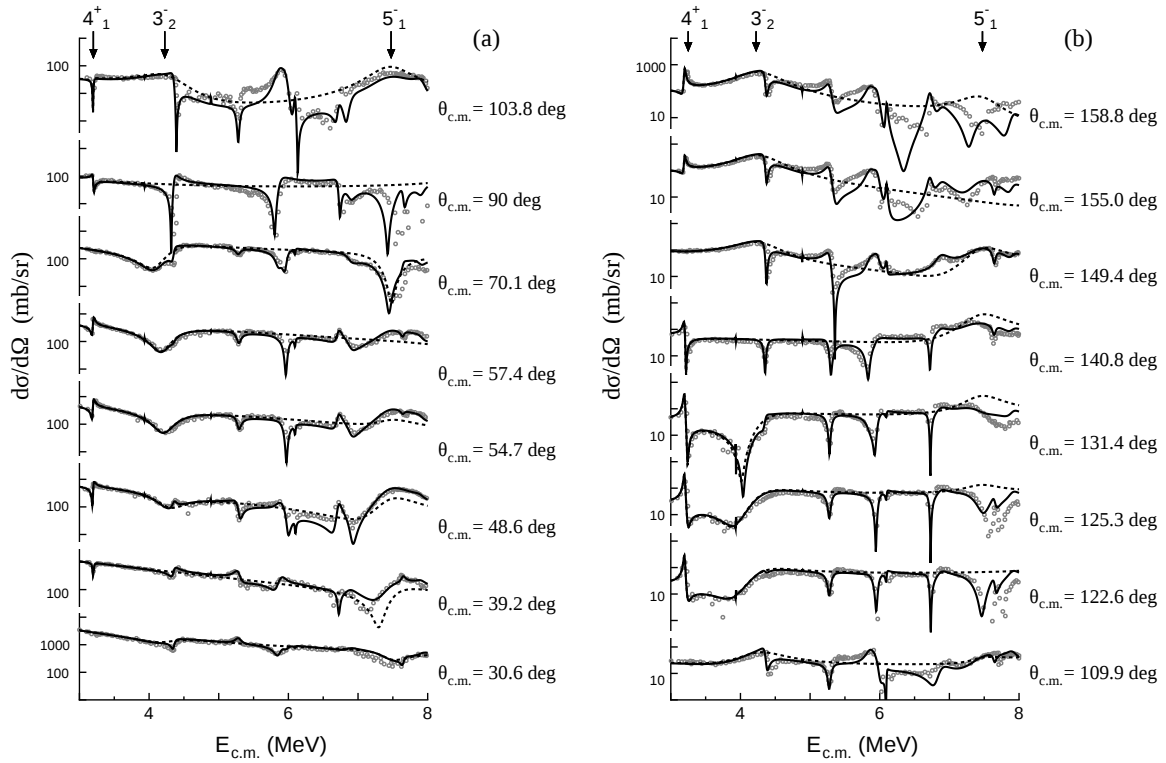


Figure 3. The excitation function of $\alpha+^{12}\text{C}$ elastic scattering in the energy region of $E_{c.m.} = 3 - 8$ MeV. The solid curves are the results obtained from the potential model with the additional resonances. The dotted curves represent the results from potential scattering. The energy position of the $\alpha+^{12}\text{C}$ rotational band [11, 12] is shown by the arrows. The scattering angles are displayed besides the respective curves. The experimental data are taken from [47, 54].

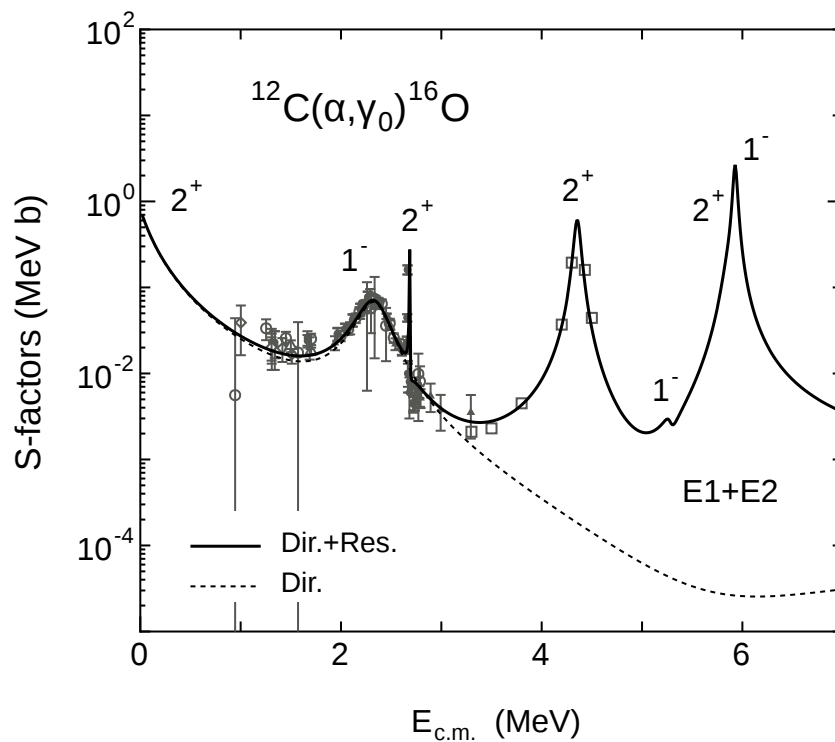


Figure 4. The astrophysical S -factors of the $^{12}\text{C}(\alpha,\gamma)^{16}\text{O}$ reaction. The solid curve is the result obtained from the potential model with the additional resonances. The dotted curve is the direct-capture component. The S -factors are the sum of the $E1$ and $E2$ transition to the ground state of ^{16}O . The experimental data are taken from [17, 18, 16, 15, 24, 19, 54].

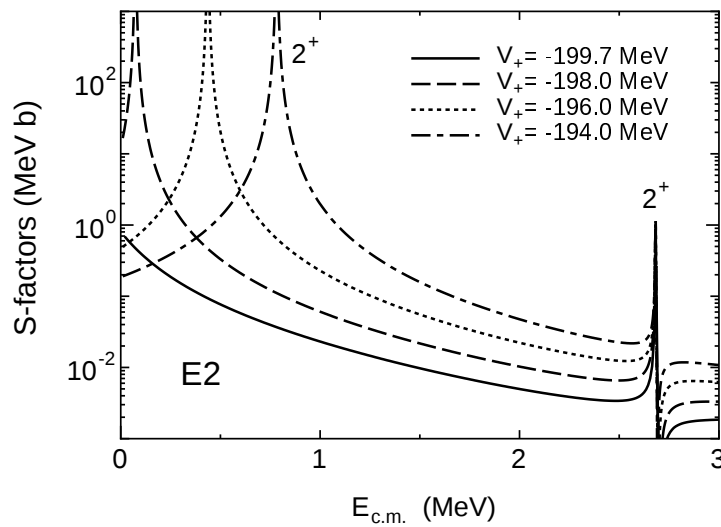


Figure 5. The schematic calculation of the $E2$ S -factors. The V_+ is varied to reveal the reason of the enhanced $E2$ S -factors. The energy position of the 2_1^+ state is shifted higher as $|V_+|$ decreases.

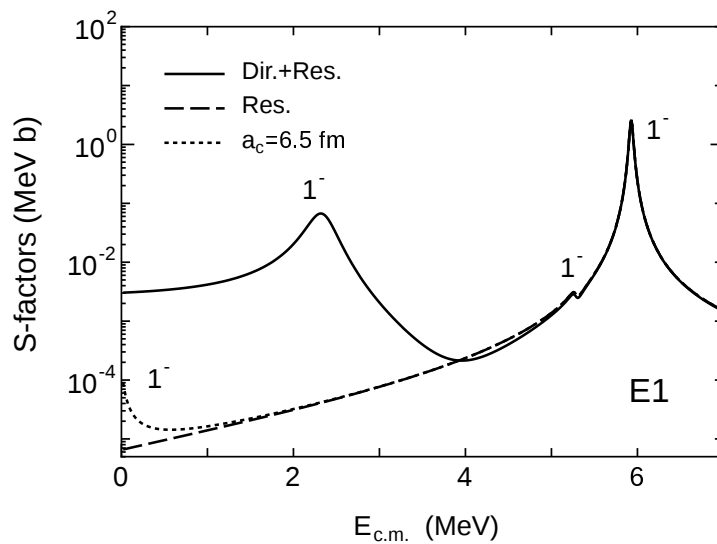


Figure 6. The $E1$ S -factors of $^{12}\text{C}(\alpha,\gamma_0)^{16}\text{O}$. The solid curve is the result obtained from the potential model with the additional resonances. The dashed and dotted curves are the components of the additional resonances. The channel radius a_c is presumed for the subthreshold state as the reference. (dotted curve)

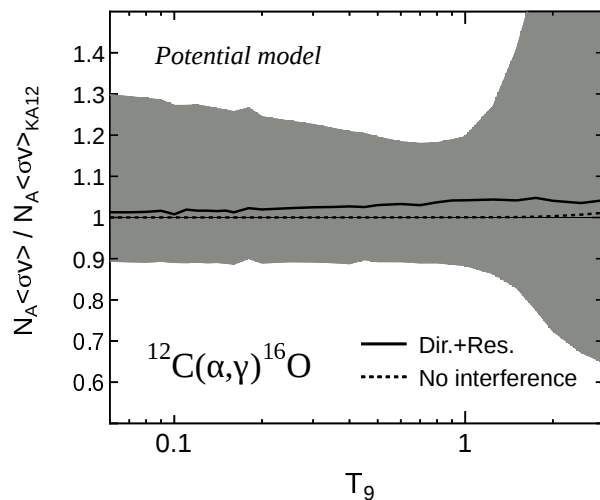


Figure 7. The thermonuclear reaction rates for the $^{12}\text{C}(\alpha,\gamma)^{16}\text{O}$ reaction. The reaction rates are displayed in the ratio to our recommended reaction rates (KA12) [2]. The solid curve is the result obtained from the numerical integration of equation (11). The dotted curve is the result with equation (12) for the resonances. The shade region is the uncertainties estimated from the variation of the model parameters. The difference from unity indicates the contribution of the additional resonances included in the present calculation.